Electronic Supplementary Information for

4D Printing Reconfigurable, Deployable and Mechanically Tunable Metamaterials

Chen Yang, Manish Boorugu, Andrew Dopp, Jie Ren, Raymond Martin, Daehoon Han, Wonjoon Choi and Howon Lee*

*Corresponding author. E-mail: howon.lee@rutgers.edu

MATERIALS AND METHODS

Materials

All chemicals including the monomer, crosslinker, photoinitiator (PI), and photo absorber (PA) were purchased from Sigma-Aldrich (St. Louis, MO, USA) and used as received. Acrylic Acid (AA) was used as a monomer and Bisphenol A ethoxylate dimethacrylate (BPA) (Mn 1700) was used as a crosslinker. The photo-curable SMP precursor solution was prepared by mixing the monomer and the crosslinker at a ratio of 55:45 in weight. Phenylbis(2,4,6-trimethylbenzoyl) phosphine and Sudan I were added at the concentration of 2 wt.% and 0.1 wt.% of the precursor solution as PI and PA, respectively.

Projection Micro-Stereolithography

A custom-built PμSL system was used in this work. It consists of a UV LED (365 nm) (L10561, Hamamatsu), a collimating lens (LBF254-150, Thorlabs), a digital micro-mirror device (DMD^{TM}) (DLPLCR6500EVM, Texas Instruments), a motorized linear stage (MTS50-Z8, Thorlabs), and a projection lens (Thorlabs). Printing parameters we used include a light intensity of 29 mW cm^{-2}, a layer thickness of 50 μm, and a curing time of 5 s. The entire PμSL system was kept in a UV blocking enclosure.

Post-processing

Printed structures were rinsed in fresh ethanol for 30 s for 3 to 4 times to remove any uncured precursor solution. Subsequently, they were dried in air until absorbed ethanol evaporated, followed by post-curing in a UV oven for 2 hours. Samples were then heated in a temperature oven at 120 ^{o}C for 12 hours to remove absorbed moisture and then kept in a dry box with desiccants until used.

Dynamic mechanical analysis (DMA)

For molded samples, a SMP precursor solution without PA was injected into a mold of two glass slides separated by 1 mm spacers. Glass slides were cleaned with ethanol and coated with trichlorosilane (Gelest, Morrisville, PA, USA) for easy demolding. The precursor solution in the

mold was cured in a UV oven (CL-1000L, UVP, 365 nm) with a light intensity of 4.4 mW cm^{-2} for 20 min, yielding a fully cross-linked polymer film with a thickness of 1 mm. Samples were laser cut to 40 mm x 8 mm x 1 mm rectangular specimens. For 3D printed samples, the same printing parameters and post-processing procedure were used. Dimensions of 3D printed samples were 25 mm x 8 mm x 1 mm. Both molded and printed specimens were heated in a temperature oven at 120 ^oC for 12 hours to remove moisture absorbed and kept in a dry box with desiccants. DMA was conducted on a dynamic mechanical analyzer (Q800, TA Instruments) using a tensile loading mode. Testing parameters for DMA included strain of 0.2 %, frequency of 1 Hz, preload of 0.001 N, and force track of 150 %. Specimens were heated at 30 ^oC for 10 min prior to each test. Storage modulus, loss modulus, and tan δ were measured as a function of temperature while temperature was increased to 90 ^oC at a rate of 1 $^oC\ min^{-1}$.

Relative density measurement

Effective density ρ_{eff} of a printed sample was measured using mass divided by total volume of the lattice. Mass was obtained using a digital scale (ML303E, Mettler Toledo). Volume was obtained by measuring length, width and height of the sample. Bulk density ρ_0 of the SMP was obtained from a 3D printed solid cylinder with a diameter of 10 mm and a height of 10 mm using the same method.

Mechanical testing

A mechanical testing system with an environmental chamber was built for mechanical testing at controlled temperature and humidity (Fig. S4A). The chamber has a clear acrylic front panel, through which a sample can be visually monitored during a test. The chamber was placed on the Peltier heater (CP-061HT, Technology, Inc.) which uses computer-controlled temperature. Temperature inside the chamber was measured using a thermocouple connected to an NI temperature module on cDAQ (NI 9171 and NI 9211, National Instrument). Dry air with ~0 % humidity was pumped into the chamber to minimize the effect of humidity. Humidity was measured using a humidity meter (iTHX-SD, Omega). A custom-machined compression plate was attached to a load cell (LCMFL-50N or LCFL-1kg, Omega) and a motorized stage (LTS150, Thorlabs). Force from load cell was recorded using an NI bridge input module and cDAQ (NI9237 and NI9171, National Instrument). Displacement was obtained by reading the position of the motorized stage. 10 min of isothermal time was given in the beginning of each test at the test temperature to ensure temperature uniformity inside the chamber and in the sample. A compression test was performed at a strain rate of 0.1 % per second for both loading and unloading. Force and displacement information obtained were converted to a stress-strain curve considering the sample dimension. Sampling frequency was 1 kHz and a smoothing method using adjacent averaging of 50 points was applied to all stress data to reduce the noise. Stiffness of a sample was obtained from the slope of the linear region of the stress-strain curve. Each sample was tested 3 times and the average stiffness was used for analysis.

Shape memory effect

Using the same mechanical testing setup, SME of the 3D printed microlattices was demonstrated. At 30 ºC, SMP microlattice was in glassy state so any mechanical deformation including compression resulted in shape programming. The microlattice was loaded to maximum strain of 85 % at a strain rate of 0.5 % strain per second, followed by unloading at the same speed. After waiting 10 minutes to allow the sample to reach an equilibrium state, the second compression with the same loading condition was applied. Shape-fixity ratio at 30 ºC was then calculated using $\varepsilon_1/\varepsilon_0$, where ε_0 is the total strain of the first compression and ε_1 is the strain that remained after the load was removed. Upon heating above glass transition temperature, SMP microlattice recovered to original shape. At 90 ºC, it was in the rubbery state and it showed an elastic behavior upon compression. The microlattice was loaded to maximum strain of 80 % at a strain rate of 0.5 % strain per second, followed by unloading at the same speed. The same loading cycle was repeated twice. Shape-recovery ratio was calculated using $1 - \varepsilon_1/\varepsilon_0$, where ε_0 is the total strain of the first compression and ε_1 is the strain that remained after the load was removed.

Impact test

An impact test was performed by dropping a mass on a SMP microlattice which was placed within a temperature oven. A metal ball with a mass of 8.6 g was painted white for enhanced visibility. The ball was released from a height of 0.6 m above the 3D printed microlattice through a transparent guiding tube. Acceleration during the impact was recorded at a sampling frequency of 2 kHz using an accelerometer (ADXL193, Sparkfun) attached underneath the rigid steel substrate on which the sample rested. Video was taken by a high-speed camera (Fastcam SA-Z, Photron) at a frame rate to 500 fps to capture the deformation of lattice during the impact.

SUPPLEMENTARY TEXT

Curing Depth Study

To determine appropriate PμSL process parameters, we studied the relationship between energy dosage and depth of cured precursor solution. The test structure consisted of two side supports and ten hanging bridges between the supports (Fig. S1A). The space between the neighboring bridges were large enough to prevent overlapping. The intensity of UV light was 29 mW cm^{-2}, and the exposure time for the bridges was increased from 0.5 sec to 9 sec. The curing depth as a function of light energy dosage was measured using a microscope and plotted in Fig. S1B. As shown in the figure, the curing depth grows as the energy dosage increases, following the stereolithography working curve equation

$$C_d = D_p ln(E/E_c) \,, \tag{1}$$

where C_d is depth of cure, and E is exposure energy. Two key constants of the precursor solution, D_p and E_c, are characteristic cure depth and critical energy required to initiate curing, respectively.[1] Based on the results, the curing time of 5 sec was chosen for the layer thickness of 50 μm.

Composition of Shape Memory Polymer

The ratio of AA and BPA for SMP was chosen such that the effective T_g of the resulting SMP was set around 65 ºC ~ 70 ºC. As a result, the SMP showed two orders of magnitude variation in modulus from 30 ºC to 90 ºC and distinctive moduli at five measured temperatures (30 ºC, 45 ºC, 60 ºC, 75 ºC, and 90 ºC). Effective T_g of a copolymer system can be estimated using Gordon-Taylor equation[2]

$$T_g = \frac{w_1 T_{g1} + k w_2 T_{g2}}{w_1 + k w_2}, \quad (2)$$

where T_g, T_{g1} and T_{g2} are the glass transition temperature of copolymer, monomer and crosslinker, respectively. w_1 and w_2 are the weight fraction of monomer and crosslinker, and k is a factor evaluated from experimental data. From DMA results of AA:BPA 50:50 shown in Fig. S2a, k was calculated to be 0.73. T_g of different ratios between AA:BPA were plotted in Fig. S2b. Based on the estimation, a ratio of AA:BPA 55:45 was chosen with an estimated T_g of 66 ºC. Estimation was verified using DMA and results were plotted in Figure 1c. Measured T_g for a molded sample in Fig. 1c was 66 ºC and for a 3D printed sample was 71 ºC.

Discrepancies in DMA results

The overall discrepancy in DMA data between the molded and 3D printed samples is attributed to the following two factors: surface roughness and light intensity. The layer-by-layer printing process inevitably introduces surface roughness to the printed object. This is also called staircase effect. When we measured dimension of the specimen to be entered in DMA, we used outer dimension. Therefore, effective dimension of the 3D printed sample was smaller than measured outer dimension. As a result, storage modulus of 3D printed samples is smaller than it is supposed to be.

We also performed FTIR scanning on the molded and 3D printed samples, along with an uncured precursor resin as a reference. The result is shown in Fig. S3. The two peaks at 1620 cm^{-1} to 1635 cm^{-1} are from the C=C bonds. The peak around 1690 cm^{-1} is from the C=O bond in acrylic acid. The peak around 1730 cm^{-1} is from the C=O bond in BPA. We normalized data with absorbance of this C=O bond in BPA as a reference because it does not participate in the polymerization reaction. First, disappearance of the peaks at 1620 cm^{-1} to 1635 cm^{-1} are observed for both molded and printed samples as the C=C bonds in the acrylates open up to form a polymer chain. The peaks of C=O around 1690 cm^{-1} shows prominent difference among the three samples. The suppression of this C=O peak progresses from the liquid resin to the molded sample to the 3D printed sample. This may suggest that the degree of conversion (DoC) of the 3D printed sample is higher than that of the molded one.

This observation is supported by a previous study,[3] which showed that higher light intensity during photopolymerization results in higher final DoC, regardless of the total energy dosage. In our experiment, light intensity of the 3D printing system was 29 mW cm^{-2}, while the UV oven

used for molding offered light intensity of only 4.4 mW cm^{-2}. Along with the FTIR analysis result, this supports our claim that DoC of the 3D printed sample is higher than that of the molded sample, which leads to higher T_g of the 3D printed sample.

Microlattice Design

An open-cell foam can be treated as a connected set of pin-jointed struts. When a load is applied on an open-cell foam, *rigidity* is defined by whether the open-cell foam allows rotation of struts about joints. A foam is called *rigid* when struts experience only axial loads (tensile/compressive) upon loading. A foam is called *non-rigid* when struts tends to rotate about joints and will not bear any load. Since joints are frictional in reality, they prevent free rotation and create bending in struts. Therefore, rigidity of an open-cell foam is determined by whether stretching or bending occurs in a strut when the foam is loaded. When *Connectivity* is defined by the number of struts connected to a joint, necessary and sufficient condition for a 3D lattice to be rigid is a connectivity of 12.[4] Since each joint is connected to 12 struts of the same length, Octet truss (OT) has a connectivity of 12 at every node, and therefore, it is *rigid*: struts in OT undergo stretching/compression upon loading (stretching-dominated). Kelvin foam (KF) consisted of 8 hexagonal surfaces and 6 planar quadrilateral surfaces. Since KF has a connectivity of 4 at each node, it is *non-rigid*: struts in KF undergo bending deformation upon loading (bending-dominated). Due to different mechanism of deformation upon loading, OT and KF microlattices show different scaling laws between relative stiffness and relative density.

The relative density $\rho_{rel} = \rho_{eff}/\rho_0$ as a function of strut length *l* and diameter *d* for an OT microlattice and for a KF microlattice (Fig. S4) is shown in Equation 3 and 4, respectively.[5,6] These two equations were used to determine length and diameter of struts for a desired relative density in CAD software, SolidWorks (Dassault Systémes, France). The scaling relations between relative stiffness $E_{rel} = E_{eff}/E_0$ and relative density $\rho_{rel} = \rho_{eff}/\rho_0$ for OT and KF microlattices are shown in Equation 5 and 6, respectively.[5,6]

$$\rho_{rel} = \rho_{eff}/\rho_0 = 1.5\sqrt{2}\pi(d/l)^2 \quad (3)$$

$$\rho_{rel} = \rho_{eff}/\rho_0 = 3\pi/8\sqrt{2}(d/l)^2 \quad (4)$$

$$E_{rel} = E_{eff}/E_0 = 1/9\left(\rho_{eff}/\rho_0\right) \quad (5)$$

$$E_{rel} = E_{eff}/E_0 = 1.007\left(\rho_{eff}/\rho_0\right)^2 \quad (6)$$

Four microlattices of each group were designed to have various relative densities (OT1~OT4 and KF1~KF4) and 3D printed with SMP using PμSL. Detailed dimensions and relative densities of the eight microlattices are listed in Table S2. *L*, *W* and *H* represent length, width and height of the printed microlattices, respectively.

Mechanical Test

To test the compressive stiffness of the SMP microlattices at different temperatures, we built a testing platform schematically shown in Fig. S5A. Detailed description of the testing platform was included in Experimental Section. Stress-strain curves of all microlattices at all temperatures are plotted in Fig. S5B. All samples showed large modulation in mechanical property with temperature. Effective compressive moduli of all samples at each temperature obtained from the stress-strain curves were used for Fig. 2C and 2D.

Impact Test

To test tunable shock absorption during an impact loading, we built an experimental setup shown in Fig. S6A. A schematic of this setup is shown in Fig. 3A in the main text. Table S3 lists design and measure parameters of the Kelvin foam microlattice used in the test. Stress-strain curves obtained at 30 ^{o}C and 90 ^{o}C were plotted in Fig. S6B. Measured modulus was 20.2 MPa at 30 ^{o}C and 0.17 MPa at 90 ^{o}C.

Reconfigurable Microlattice

For the reconfigurability test shown in Fig. 3D, we printed an OT microlattice of 2 x 2 x 6 unit cells as shown in Fig.S7. Its designed and measured parameters are listed in Table S4.

Deployable Microlattice

For the deploying test shown in Fig. 3E, we printed a KF microlattice of 3 x 3 x 7 unit cells as shown in Fig. S8. Its designed and measured parameters are listed in Table S5.

Response Time of Metamaterials

There are two aspects to be considered for the response time of a SMP microlattice: (1) time for struts to reach thermal equilibrium at a given temperature and (2) time to exhibit a temperature dependent viscoelastic relaxation (or shape recovery).

To estimate thermal equilibrium time, heat transfer in struts of microlattice needs to be considered. Assuming the temperature in the surrounding air is uniform, so no temperature gradient exists within the space and all struts in the metamaterials are subjected to the same ambient temperature. Each strut can be simplified as a 1D cylinder of radius r. It has a uniform initial temperature T_i, and then is placed into a convective heating condition with an ambient temperature T_∞. Biot number $Bi = hr/k$ indicates the relative importance between convection and conduction, where h and k are convective heat transfer coefficient and thermal conductivity, respectively. In general, if Biot number is small ($Bi < 0.1$), conduction is much faster than convection, so it can be assumed that the temperature inside the body is uniform. Based on typical convective heat transfer coefficient h of air (10 W/m^{2}K)[7], thermal conductivity of polymer k of 0.1~0.5 W/mK,[8] and the largest strut radius of our metamaterials of 350 μm, the approximated Biot number is $Bi \sim 0.035 < 0.1$, which means struts can be treated as a lumped system with uniform

temperature. Then temperature T of struts can be expressed by conductive heat transfer equation[9] as

$$T = T_\infty + (T_i - T_\infty) \cdot e^{-\frac{h}{\rho c_p}\cdot\frac{A_s}{V}t}, \quad (7)$$

where A_s is a surface area of a strut, V is a volume of the strut, and c_p is a heat capacity of the material. When the equation is written as

$$T = T_\infty + (T_i - T_\infty) \cdot e^{-\frac{t}{\tau}}. \quad (8)$$

a time constant τ can be defined as

$$\tau = \frac{\rho V c_p}{h A_s} \approx \frac{r \rho c_p}{2h}. \quad (9)$$

Using h = 10 W/m^{2}K, c_p = 1300 J/kg·^{o}C (rough estimation from PAA's heat capacity[10]), ρ = 1254 kg/m^3 (measured), and r = 3.5 x 10^{-4} m, τ can be calculated as 28.5 sec. This is a characteristic time scale of heat transfer to a strut. It should be noted that the characteristic time scale is linearly proportional to the strut radius, $\tau \sim r$.

By simple mathematical manipulation, we obtain thermal equilibrium time,

$$t = \ln\left(\frac{T - T_\infty}{T_i - T_\infty}\right) * (-\tau). \quad (10)$$

When T_i = 30 ^{o}C and T_∞ = 90 ^{o}C, the time needed for a strut having a radius of 350 μm to reach 85 ^{o}C is 70.9 sec. Thermal equilibrium time is shorter for microlattices with thinner struts for lower relative densities. For example, for KF2 having a strut radius of 170 μm, an estimated time is 34.4 sec; for OT1 having a strut radius of 45 μm, an estimated time of thermal equilibrium at 85 ^{o}C is 9.1 sec. Since thermo-responsive stiffness depends on equilibrium temperature, response time of mechanical tunability can be predicted using thermal equilibrium time.

To further explain SMP's time- and temperature-dependent viscoelastic behavior, we consider a one-dimensional linear viscoelastic model following the approach reported by Yu, *et al.* (2014) and Yuan, *et al*. (2017).[11,12] The model we used is a Generalized Maxwell model (Maxwell–Wiechert model).[13] It consists of 1 equilibrium branch and multiple non-equilibrium branches as shown in the Fig. S9. E_0 is the spring constant of the equilibrium branch, and E_i is the spring constant in i^{th} branch, and τ_i is the temperature-dependent relaxation time of a dashpot in i^{th} branch. The collective behavior due to the set of different relaxation times gives rise to the time-dependent

shape recovery of the SMP, which is the focus of 4D printing. Since these relaxation times depend on temperature, SMP's response time also varies depending on temperature.

By using the "thermorheological simplicity",[14] temperature dependence of relaxation time τ_i follows time-temperature superposition principle and can be determined by:

$$\tau_i(T) = \alpha(T)\,\tau_i^{ref}, \tag{11}$$

where τ_i^{ref} is relaxation time at a reference temperature and $\alpha(T)$ is the time-temperature superposition shift factor. Shift factor can be determined using the Williams-Landel-Ferry (WLF) equation[15]:

$$\log[\alpha(T)] = -\frac{C_1(T-T_{ref})}{C_2+(T-T_{ref})}, \qquad T > T_{ref}\ , \tag{12}$$

and an Arrhenius-type equation[16]:

$$\ln[\alpha(T)] = -AF_c k_b^{-1}\left(\frac{1}{T}-\frac{1}{T_{ref}}\right), \qquad T < T_{ref}\ , \tag{13}$$

where A is a material constant, F_c is the configurational energy and k_b is Boltzmann's constant. $AF_c k_b^{-1}$, C_1 and C_2 are material parameters. T_{ref} is the reference temperature chosen.

We used the DMA data of the 3D printed SMP specimen shown Fig. 1C to obtain spring constant E_i and relaxation time τ_i^{ref} of each branch, as well as $AF_c k_b^{-1}$, C_1 and C_2. Based on the Generalized Maxwell model, temperature dependent storage modulus $E_s(T)$, loss modulus $E_l(T)$, and $tan\delta$ can be expressed as[12]:

$$E_s(T) = E_0 + \sum_{i=1}^{n}\frac{E_i\omega^2[\tau_i(T)]^2}{1+\omega^2[\tau_i(T)]^2}\ , \tag{14}$$

$$E_l(T) = \sum_{i=1}^{n}\frac{E_i\omega\tau_i(T)}{1+\omega^2[\tau_i(T)]^2}\ , \tag{15}$$

$$tan\delta = \frac{E_l(T)}{E_s(T)}\ . \tag{16}$$

During DMA test, frequency was held constant at 1 Hz. Since T_{ref} is typically chosen 10-15 ^{o}C below T_g,[11,12] we chose 55 ^{o}C as T_{ref}. By fitting $E_s(T)$ (eq. 14) and $tan\delta$ (eq. 16) to the DMA data, we obtained E_0, E_i, and τ_i^{ref} for a Generalized Maxwell model with 1 equilibrium branch and 39

nonequilibrium branches. $E_s(T)$ and $tan\delta$ from the model and the DMA test are in good agreement as shown in Fig. S10. E_i and τ_i^{ref} for each branch and E_0 are listed in Table. S6.

With the viscoelastic material parameters available, shift factor $\alpha(T)$ as a function of temperature is determined from Arrhenius equation for $T < T_{ref}$ (eq. 12) and WLF equation for $T > T_{ref}$ (eq. 13). $\alpha(T)$ obtained in this way is shown in Fig. S11.

With the viscoelastic model, time- and temperature-dependent viscoelasticity of SMP can be estimated. For example, elastic modulus for a constant strain over time at a given temperature can be described by

$$E(t,T) = E_0 + \sum_{i=1}^{n} E_i \exp\left(-\frac{t}{\tau_i(T)}\right). \quad (17)$$

By substituting $E(t,T)$ for constituent modulus in the scaling equations of OT and KF (eqs. 5 and 6, respectively), we can obtain time- and temperature-dependent effective moduli of OT and KF for a constant strain, respectively.

$$\text{OT: } E_{eff}(t,T) = \frac{1}{9}\left(\frac{\rho_{eff}}{\rho_0}\right)\left[E_0 + \sum_{i=1}^{n} E_i \exp\left(-\frac{t}{\tau_i(T)}\right)\right] \quad (18)$$

$$\text{KF: } E_{eff}(t,T) = 1.007\left(\frac{\rho_{eff}}{\rho_0}\right)^2\left[E_0 + \sum_{i=1}^{n} E_i \exp\left(-\frac{t}{\tau_i(T)}\right)\right] \quad (19)$$

Based on the viscoelastic model, shape recovery time for the 4D printed microlattices can also be estimated. It has been shown that both viscoelastic relaxation and shape recovery of SMP follow the time-temperature superposition principle. There exists a unified parameter, reduced time t_r, that determines physical time and temperature needed for recovery or relaxation.[11] For a non-isothermal process, t_r can be determined from shift factor by:

$$t_r = \int_0^t \frac{ds}{\alpha(T)}, \quad (20)$$

where t is the physical time of the recovery process.[17] As t_r is a unified parameter, it holds constant for the thermo-temprally same recovery and viscoelastic relaxation at any temperature. With a known temperature profile, response time for viscoelastic relaxation can be predicted. For an isothermal process (deformation is released at a constant temperature), physical time t can be found by a simple relationship of $t = t_r \times \alpha(T)$.

In the shape memory effect experiment shown in Fig. 2F in the main text, KF2 was fixed at 40% of its original height and fully recovered upon heating. The total recovery time from 40% to 100% was approximately 23.3 min (1400 sec) (Movie S1). With the temperature profile during heated recovery shown in Fig. S12, t_r is found to be 3.79 x 10^5 sec. Note that we neglect heat transfer time of struts for simplicity. Using the reduced time obtained above, estimated physical

recovery time from 40% to 100% at different temperatures can be determined. It is worth noted that response time is markedly faster at higher temperature. For example, at 70 ^{o}C, the estimated physical recovery time is 848.5 sec (14.1 min). At 85 ^{o}C, the estimated physical recovery time is 14.4 sec. At 90 ^{o}C, the estimated physical recovery time is only 4.9 sec.

Response time of our 4D printed mechanical metamaterials is determined by a combination of thermal equilibrium time and viscoelastic relaxation time. For example, when KF2 with a strut diameter of 338 μm is compressed to 40% of its height and then placed at a constant temperature of 85 ^{o}C, it would take 34.4 sec for struts to reach 85 ^{o}C, and then 14.4 sec to complete full recovery of the original shape. Therefore, the estimated total response time is 48.8 sec. Note that we assume that shape recovery begins after thermal equilibrium is achieved in this estimation. In an actual heated recovery process, shape recovery and heat transfer may take place simultaneously.

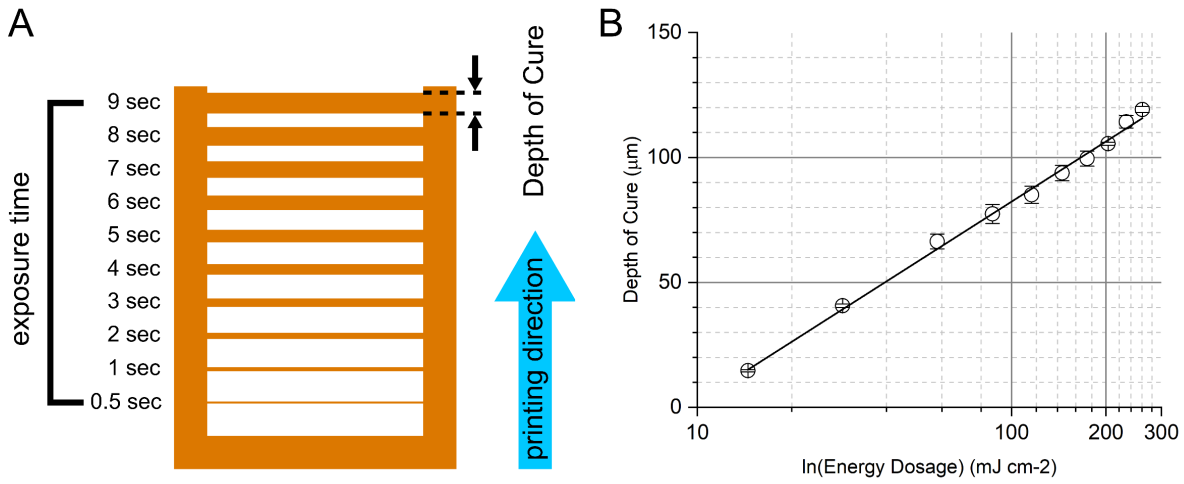

Fig. S1. (A) Schematic drawing of the test structure for curing depth study. (B) Depth of cure vs. natural log of energy dosage.

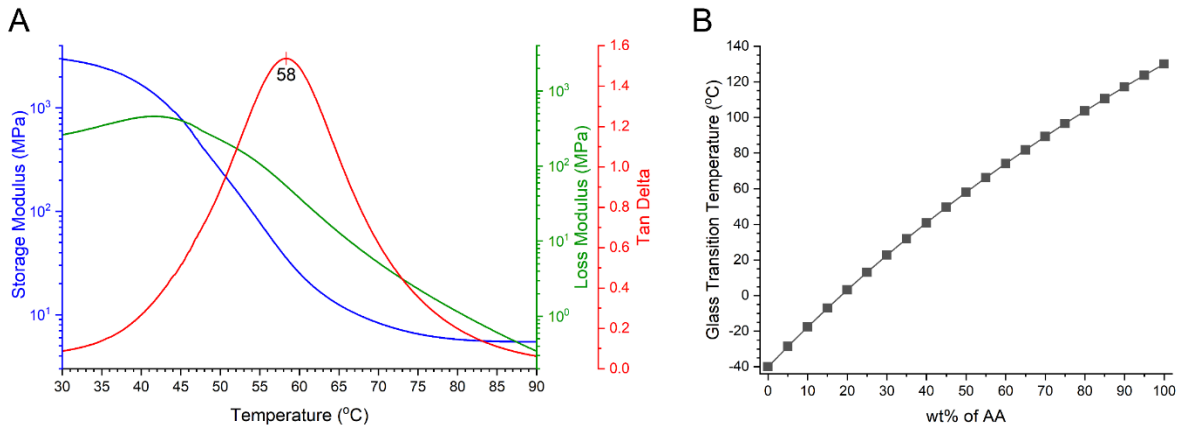

Fig. S2. (A) DMA results of AA:BPA 50:50 with a measured T_g of 58 °C. (B) Plot of estimated T_g of SMP as a function of wt.%. of AA using Gordon-Taylor equation.

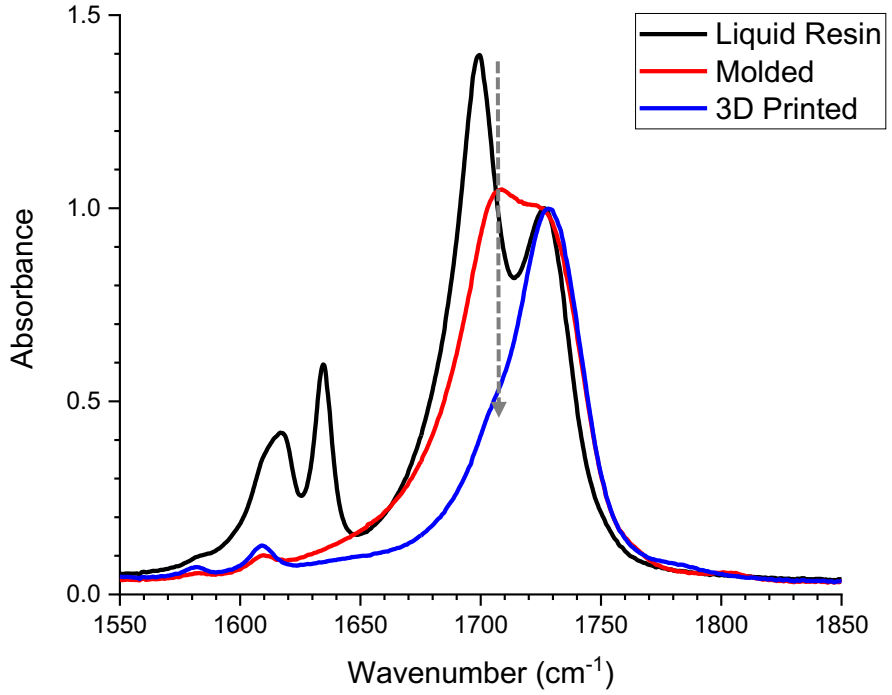

Fig. S3. FTIR results of SMP liquid resin, molded sample and 3D printed sample.

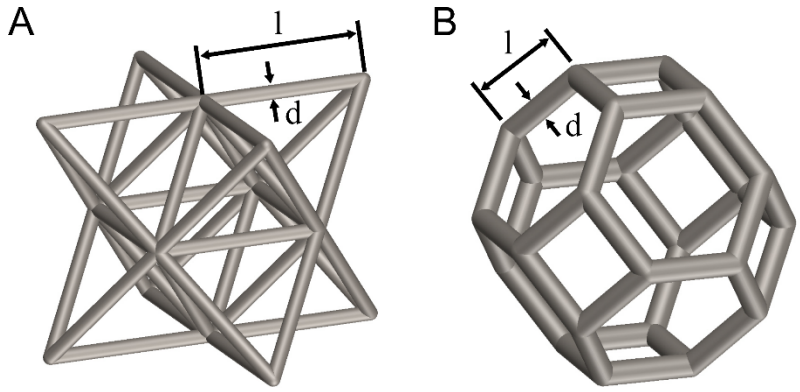

Fig. S4. (A) CAD design of a unit cell of the octet-truss (OT) microlattice. (B) CAD design of a unit cell of the Kelvin foam (KF) microlattice.

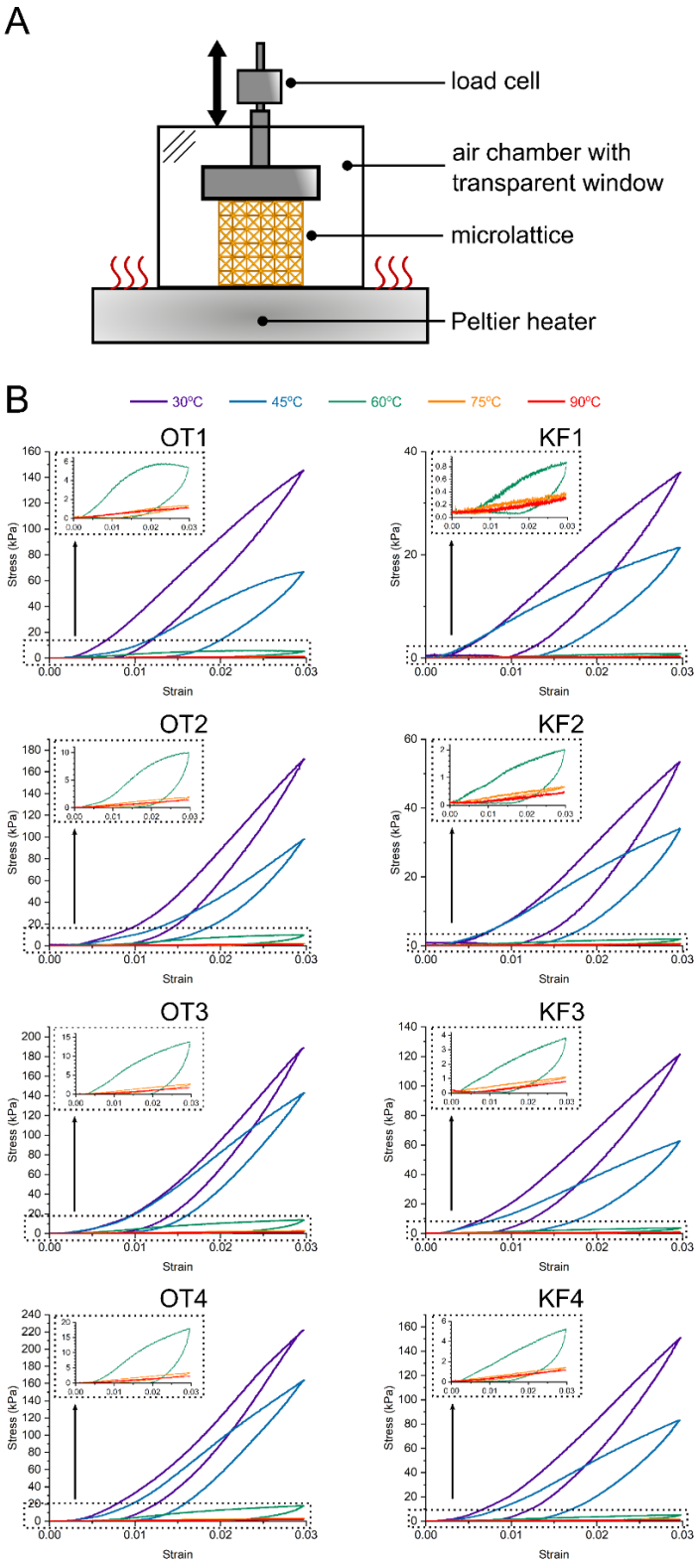

Fig. S5. (A) Schematic drawing of the test platform for mechanical test. (B) Stress-strain curves of all microlattices at all temperatures.

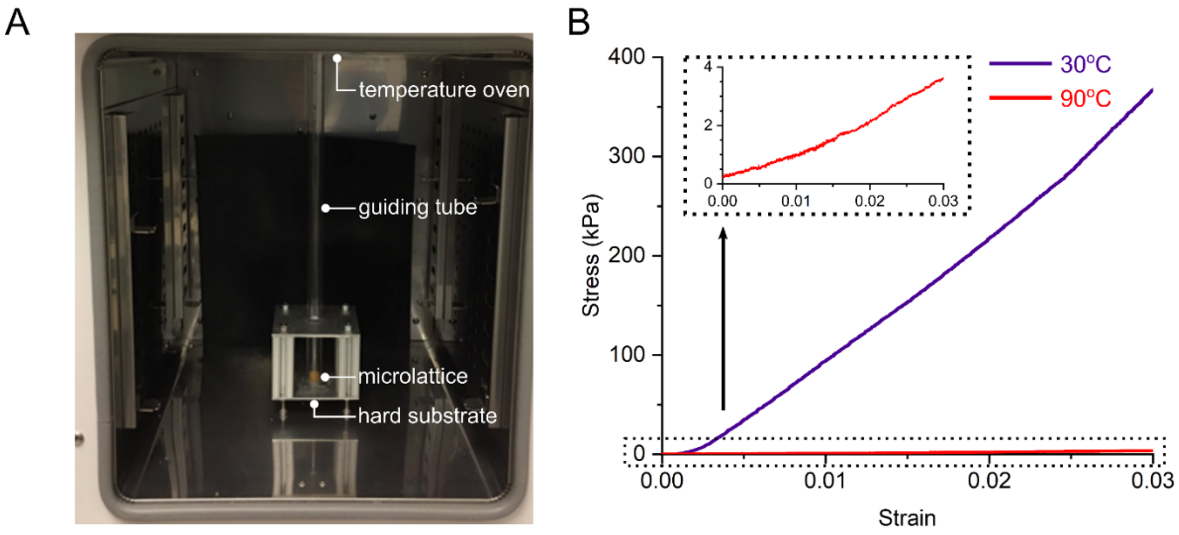

Fig. S6. (A) Picture of the impact test setup. (B) Stress-strain curves of the KF sample at 30 °C and 90 °C

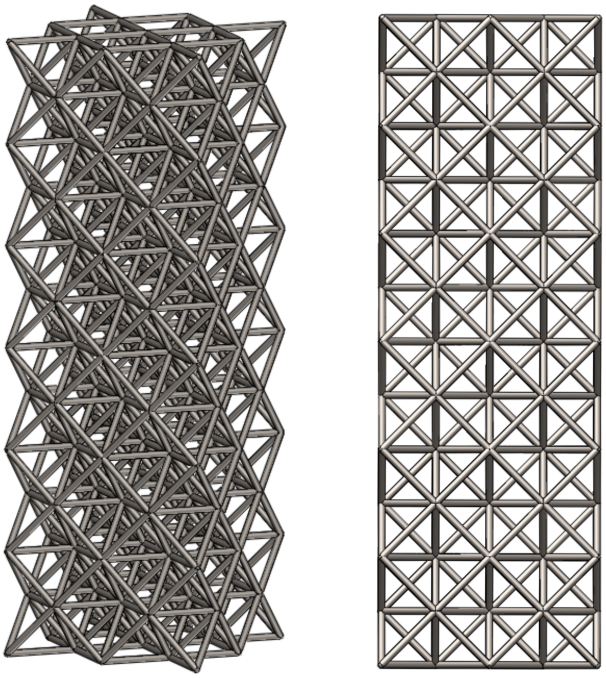

Fig. S7. CAD design of the OT microlattice in Fig. 3D

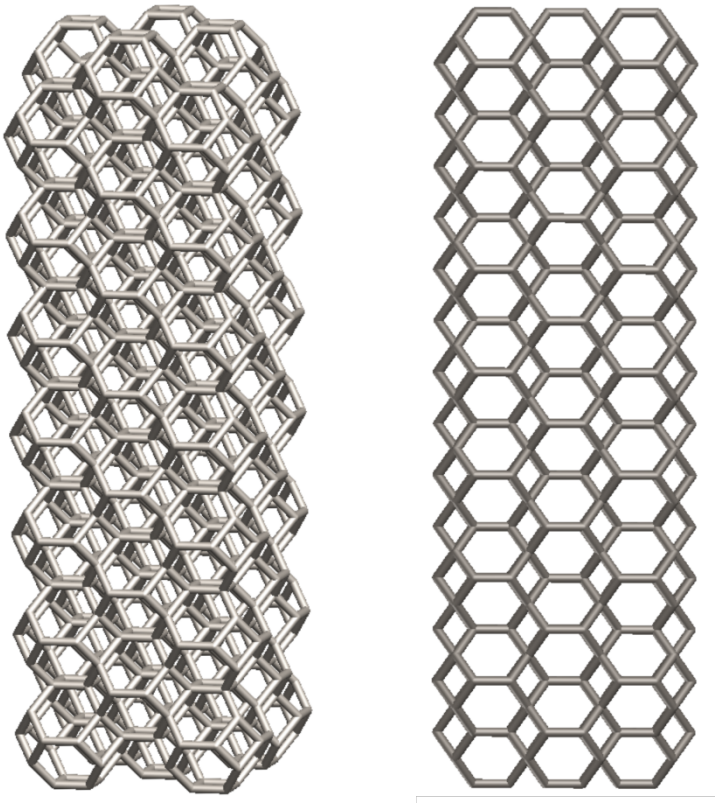

Fig. S8. CAD design of the KF microlattice in Fig. 3E

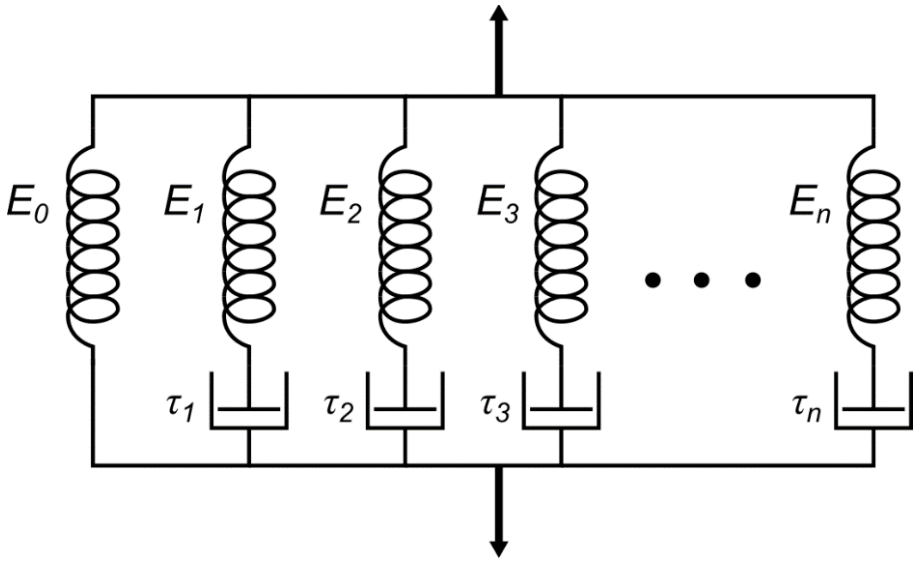

Fig. S9. 1D linear voscoelastic model

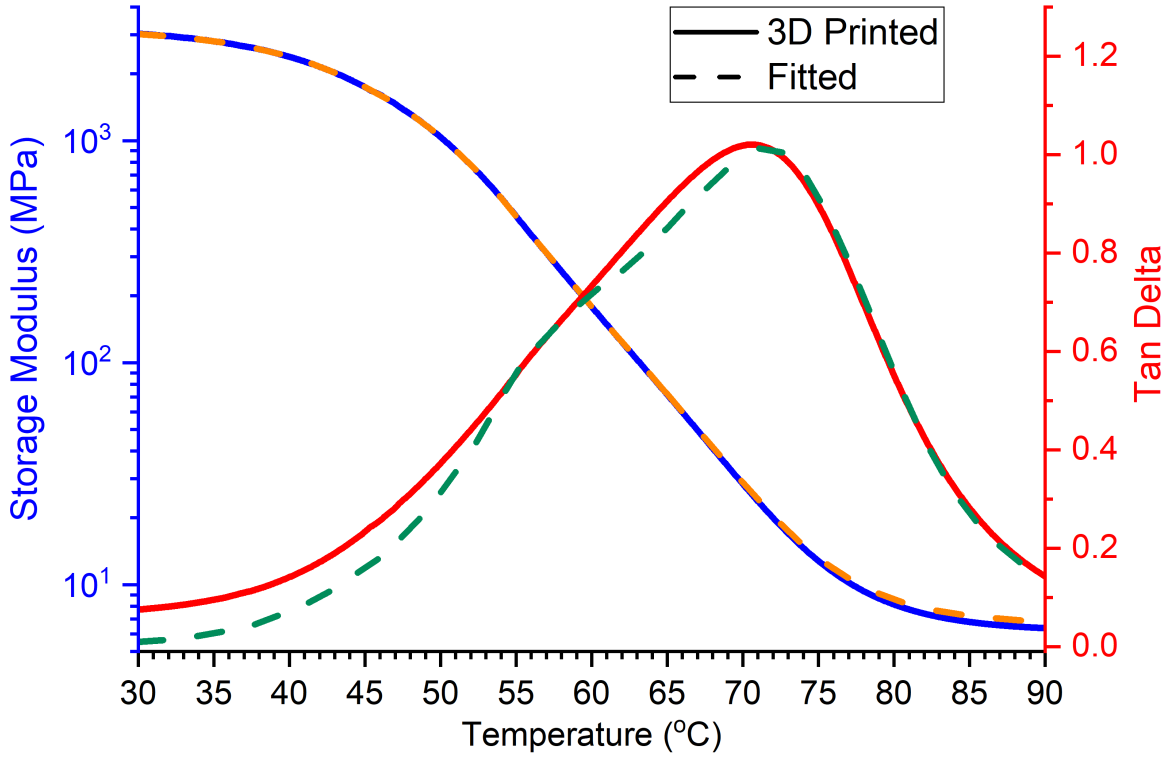

Fig. S10 Storage modulus and $tan\delta$ from DMA and the viscoelastic model

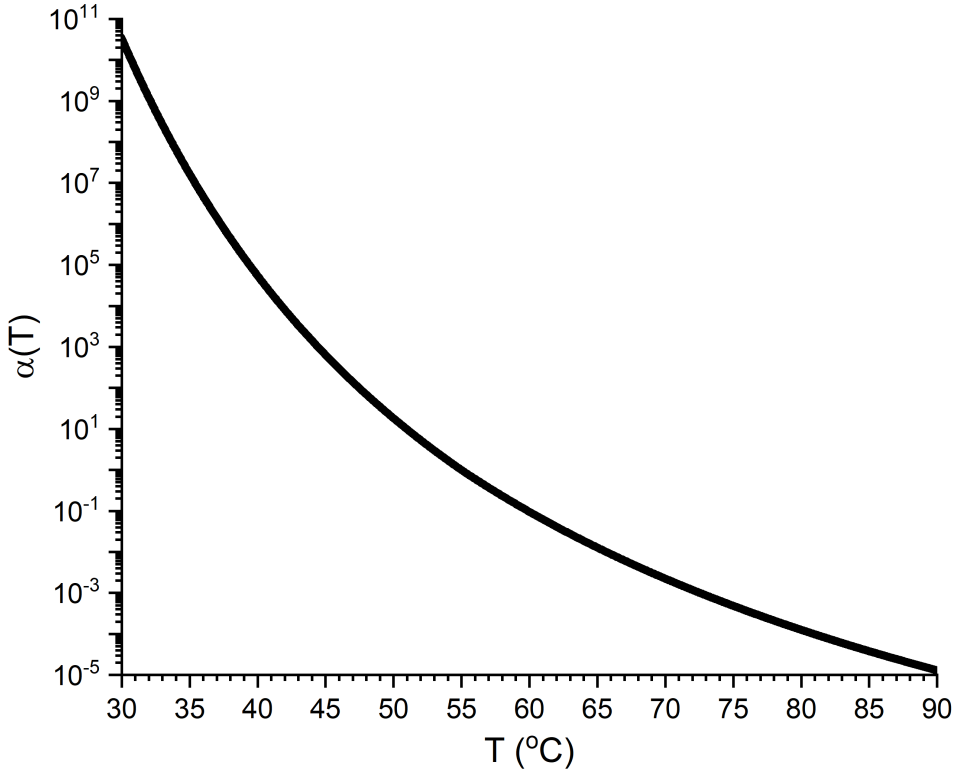

Fig. S11 Shift factor $\alpha(T)$ vs. temperature

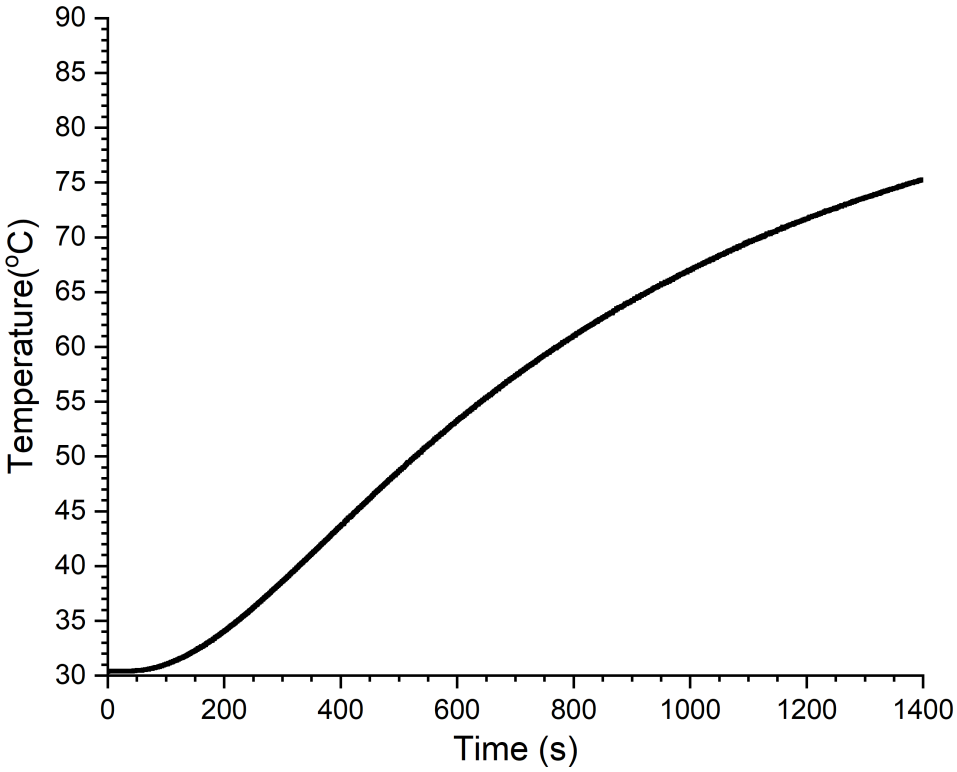

Fig. S12 Temperature profile during heated recovery in the shape memory effect experiment shown in Fig. 2F in the main text

Table S1. Measured dimensional parameters of a 3D printed SMP cylinder

	Measured Parameters				
Sample	m (g)	diameter (mm)	height (mm)	V (mm^3)	ρ_0 (g/cm^3)
Cylinder	0.981	10.5	9.74	782.3	1.25

Table S2. Designed and measured dimensional parameters of the 3D printed microlattices

	Designed Parameters			Measured Parameters					
Sample	l (μm)	d (μm)	ρ_{rel}	m (g)	L(mm)	W(mm)	H(mm)	V(mm^3)	ρ_{rel}
OT1	1380	93	3 %	0.046	9.70	9.70	9.51	894.8	4.1 %
OT2	1380	107	4 %	0.058	9.66	9.66	9.61	896.8	5.2 %
OT3	1380	120	5 %	0.072	9.64	9.64	9.62	893.9	6.4 %
OT4	1380	131	6 %	0.086	9.76	9.76	9.69	923.1	7.4 %
KF1	1380	303	4 %	0.049	9.80	9.56	10.78	1010.0	3.9 %
KF2	1380	338	5 %	0.063	9.77	9.59	10.75	1007.2	5.0 %
KF3	1380	400	7 %	0.089	9.93	9.80	10.92	1062.7	6.7 %
KF4	1380	428	8 %	0.103	9.98	9.86	10.94	1076.5	7.6 %

Table S3. Designed and measured dimensional parameters of the KF used in the impact test

	Designed Parameters			Measured Parameters					
Sample	l (μm)	d (μm)	ρ_{rel}	m (g)	L(mm)	W(mm)	H(mm)	V(mm^3)	ρ_{rel}
KF	1380	677	20 %	0.234	9.77	9.66	10.58	998.5	18.7 %

Table S4. Designed and measured dimensional parameters of the OT in Fig. 3D

	Designed Parameters			Measured Parameters					
Sample	l (μm)	d (μm)	ρ_{rel}	m (g)	L(mm)	W(mm)	H(mm)	V(mm^3)	ρ_{rel}
OT	1380	120	5 %	0.08	6.41	6.41	18.62	765.1	8.4 %

Table S5. Designed and measured dimensional parameters of the KF in Fig. 3E

	Designed Parameters			Measured Parameters					
Sample	l (μm)	d (μm)	ρ_{rel}	m (g)	L(mm)	W(mm)	H(mm)	V(mm^3)	ρ_{rel}
KF	1380	338	5 %	0.078	6.96	6.95	20.57	995.0	6.3 %

Table. S6 Parameters of the Generalized Maxwell model

T_{ref}			55		
$AF_c k_b^{-1}$			-1600		
C_1			13.3		
C_2			60.3		
E_0			6.4		
No.	τ_i^{ref}	E_i	No.	τ_i^{ref}	E_i
1	1.00E+06	1.67E-04	21	1.00E-04	1.64E+02
2	3.30E+05	1.41E-12	22	3.30E-05	1.22E+02
3	1.00E+05	4.54E-01	23	1.00E-05	1.23E+02
4	3.30E+04	3.59E-01	24	3.30E-06	9.48E+01
5	1.00E+04	1.09E+00	25	1.00E-06	6.53E+01
6	3.30E+03	3.57E+00	26	3.30E-07	8.20E+01
7	1.00E+03	9.21E+00	27	1.00E-07	5.28E+01
8	3.30E+02	2.09E+01	28	3.30E-08	4.70E+01
9	1.00E+02	3.49E+01	29	1.00E-08	4.65E+01
10	3.30E+01	5.28E+01	30	3.30E-09	3.29E+01
11	1.00E+01	8.53E+01	31	1.00E-09	3.26E+01
12	3.30E+00	1.23E+02	32	3.30E-10	2.38E+01
13	1.00E+00	2.08E+02	33	1.00E-10	3.44E+01
14	3.30E-01	2.32E+02	34	3.30E-11	1.44E-12
15	1.00E-01	2.51E+02	35	1.00E-11	4.60E+01
16	3.30E-02	2.41E+02	36	3.30E-12	4.92E+00
17	1.00E-02	2.49E+02	37	1.00E-12	9.56E+00
18	3.30E-02	1.93E+02	38	3.30E-13	6.89E+00
19	1.00E-03	2.21E+02	39	1.00E-13	1.18E-13
20	3.30E-04	1.69E+02			

REFERENCE FOR SUPPLEMENTARY INFORMATION

1 I. Gibson, D. Rosen and B. Stucker, *Additive Manufacturing Technologies: 3D Printing, Rapid Prototyping, and Direct Digital Manufacturing*, Springer-Verlag, New York, 2nd edn., 2015.
2 M. Gordon and J. S. Taylor, *Journal of Applied Chemistry*, 1952, **2**, 493–500.
3 L. G. Lovell, S. M. Newman, M. M. Donaldson and C. N. Bowman, *Dental Materials*, 2003, **19**, 458–465.
4 V. S. Deshpande, M. F. Ashby and N. A. Fleck, *Acta Materialia*, 2001, **49**, 1035–1040.
5 V. S. Deshpande, N. A. Fleck and M. F. Ashby, *Journal of the Mechanics and Physics of Solids*, 2001, **49**, 1747–1769.
6 H. X. Zhu, J. F. Knott and N. J. Mills, *Journal of the Mechanics and Physics of Solids*, 1997, **45**, 319–343.
7 Convective Heat Transfer, https://www.engineeringtoolbox.com.
8 C. Huang, X. Qian and R. Yang, *Materials Science and Engineering: R: Reports*, 2018, **132**, 1–22.
9 J. H. Lienhard, *A Heat Transfer Textbook: Fourth Edition*, Courier Corporation, 2013.
10 Poly(acrylic acid), https://polymerdatabase.com.
11 K. Yu, Q. Ge and H. J. Qi, *Nature Communications*, 2014, **5**, 3066.
12 C. Yuan, Z. Ding, T. J. Wang, M. L. Dunn and H. J. Qi, *Smart Materials and Structures*, 2017, **26**, 105027.
13 D. Gutierrez-Lemini, *Engineering Viscoelasticity*, Springer US, 2014.
14 M. Rubinstein and R. H. Colby, *Polymer Physics*, OUP Oxford, 2003.
15 M. L. Williams, R. F. Landel and J. D. Ferry, *J. Am. Chem. Soc.*, 1955, **77**, 3701–3707.
16 E. A. Di Marzio and A. J. M. Yang, *J Res Natl Inst Stand Technol*, 1997, **102**, 135–157.
17 G. W. Scherer, *Relaxation in Glass and Composites*, Krieger Publishing Company, 1992.

Movie S1:

Shape programming of SMP microlattices at 30 ºC and shape recovery of SMP microlattices upon heating to 90 ºC.

Movie S2:

Impact test on the SMP KF microlattice at 30 ºC and 90 ºC.

Movie S3:

A SMP KF microlattice was programmed to have a smaller dimension to navigate through a narrow channel and was deployed using shape recovery to regain its load-bearing capability.